JOURNAL OF PROPULSION AND POWER
Vol. 12, No. 4, July–August 1996

Correlation of Slag Expulsion with Ballistic Anomalies in Shuttle Solid Rocket Motors

Jay K. Sambamurthi* and Alexis Alvarado†
NASA Marshall Space Flight Center, Huntsville, Alabama 35812
and
Edward C. Mathias‡
Thiokol Corporation, Brigham City, Utah 84302

During the Shuttle launches, the solid rocket motors (SRM) occasionally experience pressure perturbations (8–13 psi) between 65–75 s into the motor burn time. The magnitudes of these perturbations are very small in comparison with the operating motor chamber pressure, which is over 600 psi during this time frame. These SRM pressure perturbations are believed to be caused primarily by the expulsion of slag (aluminum oxide). Two SRM static tests, TEM-11 and FSM-4, were instrumented extensively for the study of the phenomena associated with pressure perturbations. The test instrumentation used included nonintrusive optical and infrared diagnostics of the plume, such as high-speed photography, radiometers, and thermal image cameras. Results from all of these nonintrusive observations provide substantial circumstantial evidence to support the scenario that the pressure perturbation event in the Shuttle SRM is caused primarily by the expulsion of molten slag. In the static motor tests, the slag was also expelled preferentially near the bottom of the nozzle because of slag accumulation at the bottom of the aft end of the horizontally oriented motor.

Introduction

THE Space Shuttle utilizes nearly six million pounds of the combined boosting power of two solid rocket motors (SRMs) during its launch into low Earth orbit. Since the redesign of the SRM and the return to flight in September 1988, 43 pairs of the redesigned solid rocket motor (RSRM) have been successfully fired in the launching of the Space Shuttle. Additionally, during the redesign effort, 22 successful static firings of the SRMs have been conducted at the Thiokol Space Operations test facility in Utah to verify and qualify the improvements to the motor. After completion of the redesign efforts and refurbishment of postlaunch motor components, RSRM has been redefined as a reusable solid rocket motor.

During the STS-54 launch (RSRM-29) on Jan. 13, 1993, the right-hand solid rocket motor experienced a 13.9-psi chamber pressure perturbation at 67 s into the motor operation[1] (Fig. 1). This pressure augmentation equated to a thrust change of about 51 klb, and in combination with a 1 m in. bias in the burning rate of the propellant in the right motor over that in the left motor resulted in a derived thrust imbalance of 76 klb. Historically, several Shuttle solid rocket motors flown to date have exhibited pressure perturbations during the 65- to 75-s period after the motor ignition. However, all thrust and pressure variations (including the STS-54) have remained within the specification limits. Postflight assessment of the motors has not revealed any anomalous conditions.

Pressure perturbations have been observed in other solid rocket motors caused from the expulsion of igniter or insulation materials,[2–4] and the motor thrust during such events drops abruptly before rising. However, the RSRM motors do not exhibit such behavior during chamber pressure perturbation events. Instead, the thrust increases with the chamber pressure and at a higher rate than the chamber pressure when sampled over the relatively long duration of the pressure perturbation event.[5] The resulting ratio of the thrust to pressure ratio $[(F/P)_{\text{measured}}/(F/P)_{\text{expected}}]$ is greater than 1.0, indicating an augmentation of the thrust during the perturbation event over and above that associated with the chamber pressure rise. The observed time span of these pressure perturbations, lasting over a second, is also much longer than expected for an object such as insulation or other solid debris exiting the nozzle.

Several scenarios were investigated to explain the pressure perturbations in the RSRMs based on a fault tree developed after STS-54. Of these, the expulsion of slag appeared to be the most plausible scenario[6] to explain the observations in the chamber pressure as well as the thrust-to-pressure ratio increase. The ballistic effects of ejection of a continuous stream of slag debris were evaluated using simple one-dimensional nozzle ballistic models by Whitesides.[5] Condensed-phase aluminum oxide (Al_2O_3), referred to as slag, is a natural combustion product of aluminized solid rocket propellant.[7,8] The Shut-

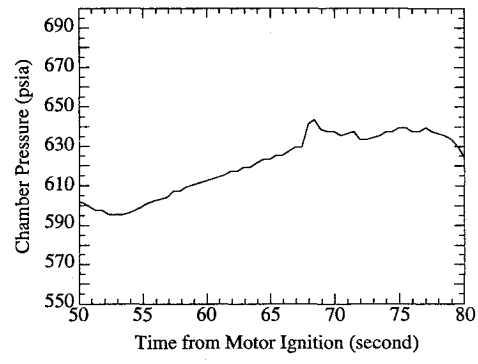

Fig. 1 Chamber pressure perturbation in right-hand RSRM during STS-54 launch.

Presented as Paper 95-2723 at the AIAA/ASME/SAE/ASEE 31st Joint Propulsion Conference and Exhibit, San Diego, CA, July 10–12, 1995; received Aug. 31, 1995; revision received Dec. 21, 1995; accepted for publication Jan. 6, 1996.

*Aerospace Engineer, M/S ED33. Senior Member AIAA.
†Aerospace Engineer, M/S ED64.
‡Principal Engineer, Space Operations. Member AIAA.

tle RSRM propellant contains 16% aluminum by weight. In the RSRM, the cavity created by the submerged portion of the nozzle in the motor's aft end (Fig. 2) provides an ideal location for slag accumulation during motor burn. This slag mixes with the recirculating gaseous combustion products of the propellant and forms a slurry. Ejection of this slurried slag mass may be induced by nozzle vectoring, unsteady gasdynamic phenomena, or lateral vehicle accelerations, resulting in a chamber pressure perturbation. Hopson[9] using a fluid/structural model of the RSRM aft cavity, developed a slosh model for the slag pool in the 60- to 80-s time frame and identified throughout the RSRM flight program a lateral acceleration component in the flight data during the same time frame that acted as a forcing function for the slag pool sloshing. Also, recent studies with the cold flow ejection model by Whitesides et al.[10] suggests that an unsteady, turbulent flow effect is operative in the periodic slag ejection events.

Two full-scale motor static firings, technical evaluation motor no. 11 (TEM-11) and flight support motor no. 4 (FSM-4) were instrumented extensively to further understand the slag expulsion phenomenon in the RSRM and the associated chamber pressure perturbations. In both tests the instrumentation for nonintrusive optical and infrared (IR) diagnostics of the plume included high-speed photography, radiometers, and thermal image cameras, in addition to other instruments, such as real time radiography (RTR), accelerometers, strain and girth gauges, and thermocouples. This article describes the optical and IR instrumentation employed in the two static firings: 1) the observations from these instruments and 2) the interpretations to support the scenario that slag expulsion causes the pressure perturbation events in the RSRM.

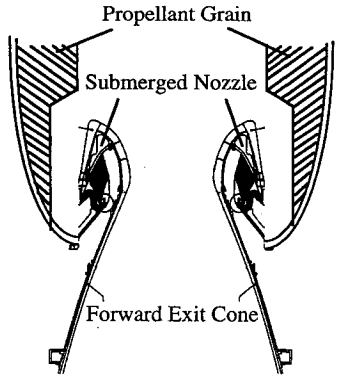

Fig. 2 Submerged RSRM nozzle.

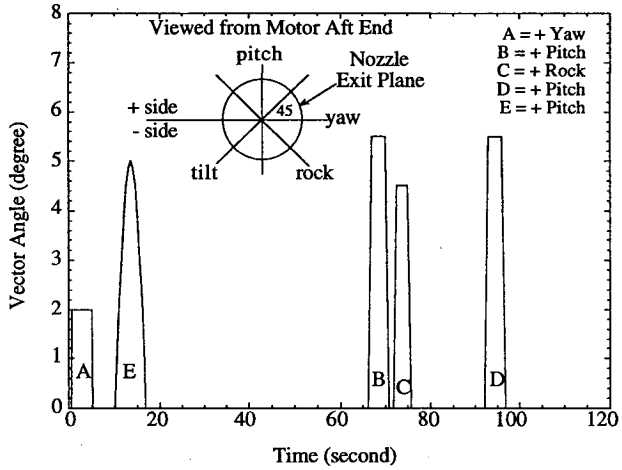

Fig. 3 Nozzle vectoring in TEM-11 and FSM-4 test (event *E* was employed in FSM-4 only).

SRM Static Test

The static firing of a full-scale SRM is normally conducted on one of the two test stands, T-24 and T-97, at the Thiokol Space Operations test facility at Promontory, Utah. TEM-11 was fired on Sept. 28, 1993 in T-97, and FSM-4 was fired on March 10, 1994 in T-24. TEM-11 was a high-performance motor with mostly Kerr–McGee (KM) ammonium perchlorate (AP) propellant, and FSM-4 was an RSRM with Western Electrochemical Company (WECCO) AP propellant.

During the static firing, the motors were oriented horizontally with the motor centerline 10 ft above the ground. This orientation is favorable for slag accumulation in the submerged nozzle region of the motor, as evidenced by the slag retained at the end of the motor burn, and indicated by the RTR.[11,12] To induce expulsion of the accumulated slag and the associated phenomenon in the chamber pressure, unique nozzle vectoring (Fig. 3) was employed in both static firings. Vectoring event *E* was added to the FSM-4 duty cycle to determine if a pressure perturbation could be induced early in the burn with the absence of any accumulated slag in the motor's aft end.

Instrumentation

The motor plumes were visually observed using high-speed cameras at rates of both 1000 and 2000 frames/s. Five cameras were employed in the TEM-11 and four cameras in the FSM-4 test. The cameras, located about 300 ft from the nozzle, observed the plume from the nozzle exit plane to about five nozzle diameters downstream. All cameras were located aft of the nozzle exit plane, and were turned on remotely at 60 s after motor ignition. The 1000-frames/s camera filmed the plume until 108 s after motor ignition, whereas the 2000-frames/s camera filmed the plume until 84 s after motor ignition. The frame exposure times of these high-speed cameras ranged from 1/5000 to 1/10,000 s.

Figure 4 shows the radiometer arrangement employed in the TEM-11 static firing to study the pressure perturbation analysis. Wide-angle radiometers were mounted directly on the nozzle wall and aimed parallel to the plume axis. These radiometers provided a circumferential distribution of the plume radiation during the pressure perturbation events. The 4-deg, narrow-view radiometers were mounted on a post downstream of the nozzle exit plane to measure radiation across the plume at a location 45 in. downstream from the nozzle exit plane. These radiometers were collectively mounted 10 ft above the test bay floor (same height as the nozzle centerline) and aimed as indicated in Fig. 4. Two sets of specially designed 50-deg wide-angle radiometer pairs, with a higher response (15 ms), were also employed in this test to identify the nature of the emissions in the plume during the pressure perturbation events. Each pair included one radiometer with an external sapphire window and another with both an external sapphire window and a 1.45- to 1.85-μm filter underneath. The radiometers were aimed at the target location using a laser beam and a crosshair mounted on a pole. The accuracy of the pointing procedure was estimated to be within ± 1 in. of the target location.

The radiometer arrangement for the FSM-4 test was identical to that in the TEM-11 test, except for the following: the specially designed 50-deg wide-angle radiometer pair was removed from station 1881.40 and mounted on the test bay floor 1 ft above the ground and 8 ft forward of the nozzle exit plane, and aimed aft toward the plume 1 ft below the nozzle lip. The 4-deg, narrow-view radiometers were deleted. Instead, four narrow-view radiometers (6 deg) were mounted on the nozzle external wall every 90 deg, starting at 3 deg and at a station 6 in. forward of the nozzle exit plane.

The nozzle-mounted 150-deg wide-angle radiometers, as well as the 4- and 6-deg narrow-view radiometers, were 0–100 Btu/ft^2-s gauges with a measurement accuracy of $\pm 3\%$. The response time of the 150-deg wide-angle radiometer was about 300 ms, and that of the narrow-view radiometer was

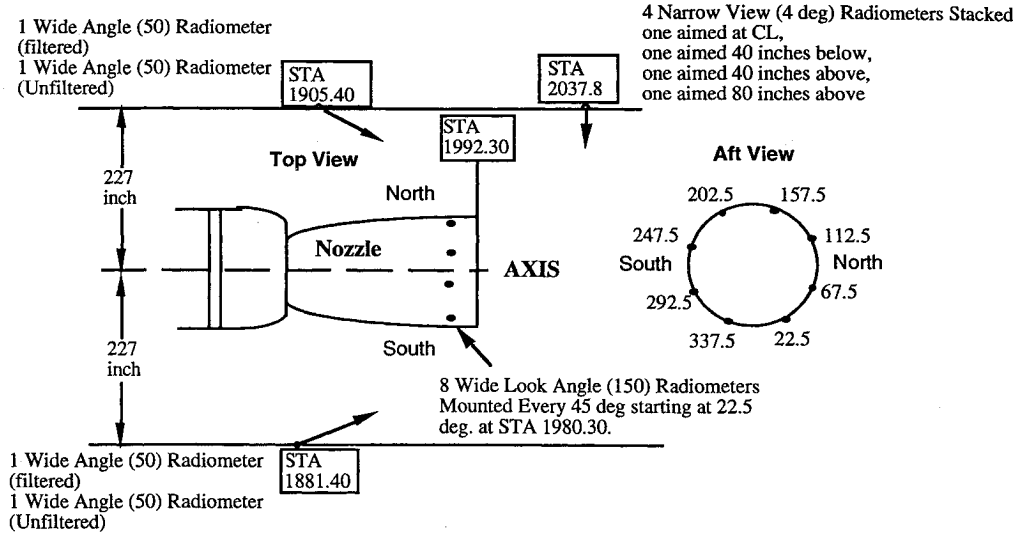

Fig. 4 Radiometer arrangement in TEM-11 test to support pressure perturbation studies.

about 1 s. The 50-deg wide-angle radiometer had a range of 0–20 Btu/ft^2-s and the same accuracy level as other radiometers.

IR cameras were also employed in the two tests to observe the plume in the 3- to 12-μm range at a scanning rate of 30 frames/s. The cameras were located about 300 ft from the nozzle and about 80–120 ft forward of the nozzle exit plane. In the TEM-11 test, two thermal image cameras were located on the south side of the motor. For FSM-4, thermal image cameras were located on both sides of the motor. The cameras used included an Inframetrics 760 and an Inframetrics 600. The temperatures measured by these cameras were accurate to within $\pm 2\%$. The purpose of these cameras was to study the nature of the thermal emissions from the ejected material during the pressure perturbation events.

Efforts to study the plume with a spectrometer in the 1- to 12-μm range were not successful. The change in the shape of the spectrum during the pressure perturbation, in conjunction with the results of the thermal image cameras and the 50-deg view-angle radiometers, would have provided further insight into the nature of the ejected material.

Results

The chamber pressures measured at the head end of the motor for both TEM-11 and FSM-4 tests are illustrated in Figs. 5a and 5b. The nozzle vectoring employed in the two tests is also shown here. As mentioned before, nozzle vectoring event *E* was performed only in the FSM-4 test. As anticipated, pressure perturbations occurred during the 66–70-s nozzle pitch-up event in both tests. The magnitude of the pressure perturbation was about 11 psi in the TEM-11 test and 9.1 psi in the FSM-4 test. Both tests peaked at about 68 s and lasted for about 1.5 s. The pressure perturbations in the succeeding rock vectoring event for both tests were in the 5-psi range, and were significantly smaller compared to the pressure perturbation events at 68 s. Also, as expected, there was no evidence of a chamber pressure perturbation during event *E* in the FSM-4 test. However, in the FSM-4 test, a pressure perturbation of approximately 8 psi occurred near web time (109.3 s) without any nozzle vectoring.

Analyses of the high-speed motion pictures of the plume from both the TEM-11 and FSM-4 tests in the 60- to 108-s time frame clearly demonstrated the expulsion of hot, bright material in the vicinity of the bottom of the nozzle exit plane during the chamber pressure perturbation events. Typical ejecta from the TEM-11 test before and during the 68-s pressure perturbation event are illustrated in Figs. 6a and 6b. These observations were made in both the TEM-11 and FSM-4 tests.

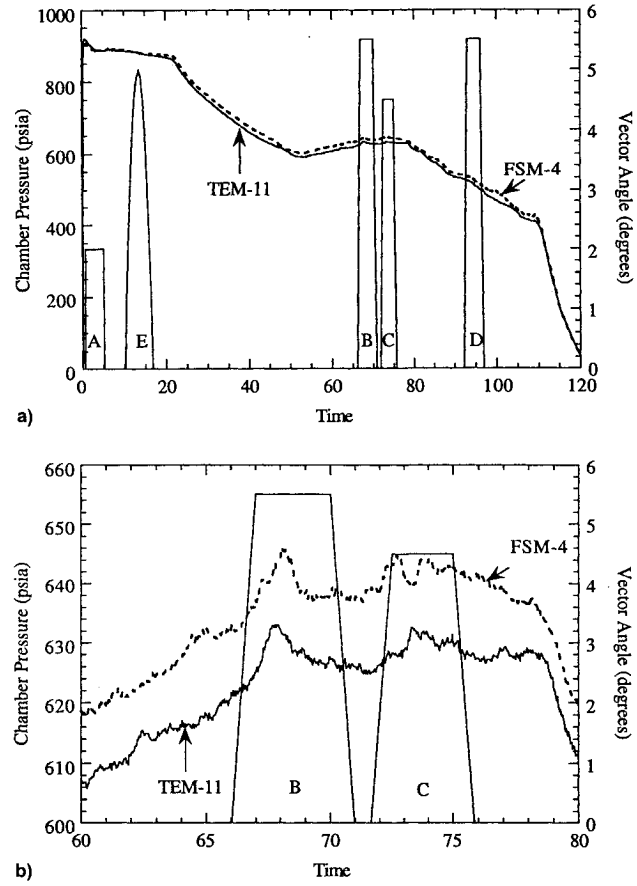

Fig. 5 Chamber pressure traces for a) TEM-11 and FSM-4 tests and b) in the 60- to 80-s time frame for TEM-11 and FSM-4 tests showing pressure perturbations during vectoring events *B* and *C*.

These ejecta were highly localized lasting for fractions of a second and appeared as bright, white streaks. The white streaks in the high-speed film (their shape, motion, and brightness), suggest a more dense fluid, such as slag.[12] These white streaks were predominantly observed at the bottom of the plume. When the high-speed film indicated an increase in white streak activity, the radiometers nearest the activity showed an increased heat flux, and there was also an increase of the motor head-end pressure during that period of time. The larger the area covered by the white streaks, the more the radiometer

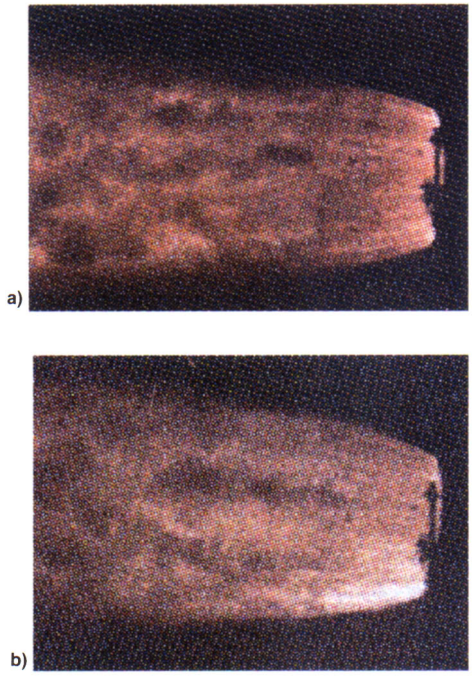

Fig. 6 a) Quiescent plume at 66 s in TEM-11 test (before nozzle vectoring event *B*) and b) localized white streak near bottom of nozzle during 11-psi pressure perturbation at 68 s in TEM-11 test.

responded. The heat flux responses of the radiometers on the nozzle are discussed in the following paragraphs. The angular position of the streaks also matched the location of the increased heat flux measured by the radiometers. The highly agitated motion of the slag in the vicinity of the nozzle lip (observed on the RTR) prior to the pressure perturbation events also strongly indicated that the pressure perturbations were caused by slag ejection.[11,12]

Figures 7a and 7b show the radiation measured by the wide-angle radiometers mounted on the nozzle external wall on the north side of the vertical axis (pitch plane) in the TEM-11 test. The chamber pressure is also shown in these figures. The radiometers mounted on the top half of the nozzle (UANAV003 and UANAV004) were quiescent during the entire motor burn and followed the nominal motor chamber pressure trace. However, the radiometers mounted on the bottom half of the nozzle (UANAV001 and UANAV002) were considerably noisier from 40 s after the motor ignition to the end of the motor burn. These radiometers also measured distinct radiation spikes, matching very well with the pressure perturbation events in the motor, with almost one-to-one correspondence, as shown in Fig. 7b. These radiation spikes also matched well with the increased hot, white emission activities observed in the bottom half of the plume in the high-speed motion pictures. Similar observations were made in the measurements of the wide-angle radiometers mounted on the other half of the nozzle (symmetric about the vertical axis) in the TEM-11 test, as well as the nozzle-mounted radiometers in the FSM-4 test.

Figure 8 illustrates the heat fluxes measured by the wide-angle radiometers (UANAV001 and UANAV008), mounted on the nozzle at 22.5 and 337.5 deg, respectively, in the TEM-11 test. These two radiometers were located symmetrically about the pitch plane of the nozzle (vertical axis) as shown in Fig. 8. Both of these radiometers measured heat flux spikes during the 11-psi pressure perturbation associated with pitch event *B*, since slag ejection associated with the pitch vectoring would have been in the plane of symmetry of these two radiometers. However, during rock event *C*, the nozzle inlet nose cap moved toward the submerged nozzle region at the 45-deg angular location. This motion induced the localized ejection of the slag into the plume toward the rock plane of the nozzle

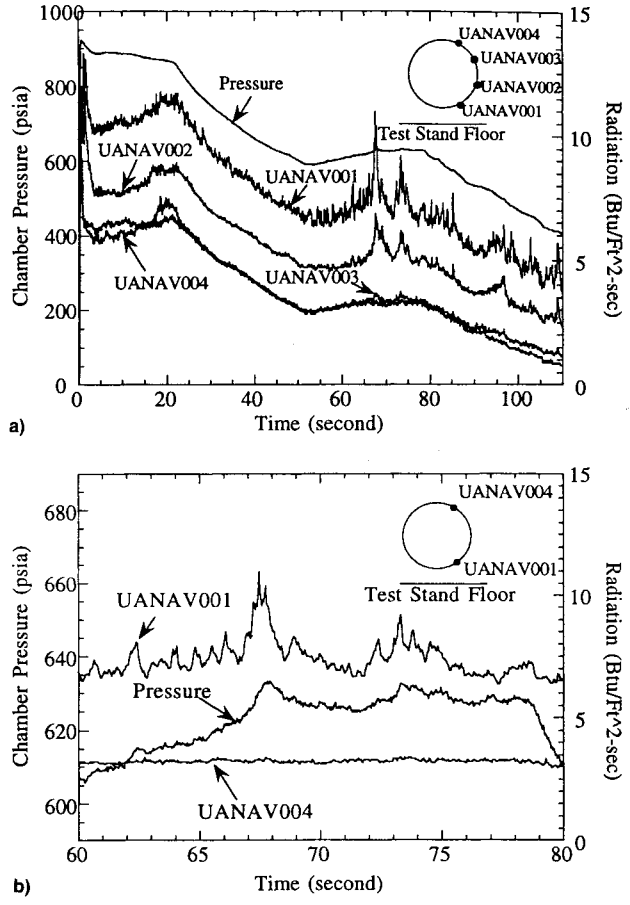

Fig. 7 a) TEM-11 nozzle wall radiometer heat fluxes for different circumferential location gauges and b) distinct heat flux perturbations by radiometer mounted in nozzle bottom half during chamber pressure perturbation events in TEM-11 test.

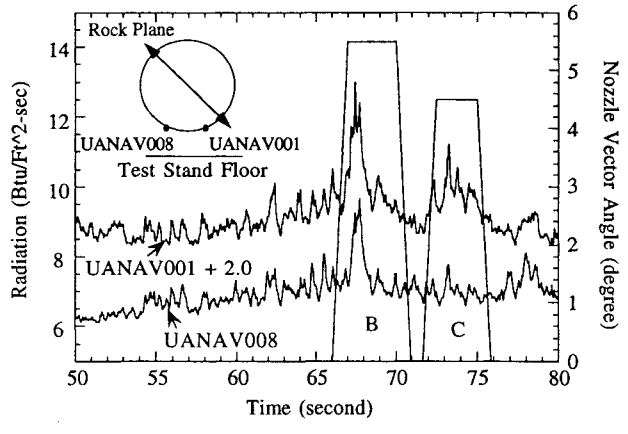

Fig. 8 Comparison of nozzle-mounted radiometer measurements during rock event *C* in TEM-11 test.

and the associated 5-psi pressure perturbation. Consequently, a significant radiation spike was measured by the radiometer located at 22.5 deg (UANAV001), whereas no appreciable radiation spike was measured by the radiometer located at 337.5 deg (UANAV008). For FSM-4, the radiometer located at 22.5 deg was sooted and read low during rock event *C*. However, the 67.5-deg gauge recorded a higher heat flux than the 337.5-deg gauge.[12] Such radiometer observations clearly demonstrated that dipping the nose of the nozzle into the submerged nozzle region at the 45-deg angular location would cause the slag to be expelled toward that plane, resulting in a chamber pressure perturbation. These results support the localized na-

ture of the slag emissions during the nozzle vectoring events and the associated chamber pressure perturbations in the motor.

Similar radiation spikes corresponding to the pressure perturbations were also observed in the measurements of the 4-deg, narrow-view radiometers (Fig. 9), mounted on the post downstream of the nozzle exit plane in the TEM-11 test. Radiometer URPAX010, aimed 40 in. below the plume centerline, measured the radiation spikes associated with the pressure perturbations during the nozzle vectoring events. However, radiometers URPAX052 and URPAX051, aimed 40 and 80 in. above the plume centerline, did not measure any corresponding radiation spikes. These results were consistent with the observations from the nozzle-mounted radiometers and add further evidence to the localized ejection of hot slag material in the bottom half of the plume during the pressure perturbation events. Moreover, the radiation spike measured by radiometer URPAX010 during the pressure perturbation associated with rock event *C* was larger than the radiation spike during the pressure perturbation associated with pitch event *B*. This result should be expected as this radiometer viewed the plume from the north side, which was closer to the rock plane of the nozzle, and the slag was expected to have a preferred ejection location through the nozzle toward the nozzle vectoring plane.

The thin film sensors used in the 50-deg high-response (15 ms) radiometers in the TEM-11 test failed during the test because of the strong ground vibrations. These sensors were redesigned for the FSM-4 test at a reduced response time of 30 ms. They then functioned nominally. The radiation measured by these paired radiometers was intended to be utilized in conjunction with other radiometer and spectrometer data to provide further circumstantial evidence that the material ejected by the SRM during the pressure perturbation events was slag (aluminum oxide) accumulating inside the motor.

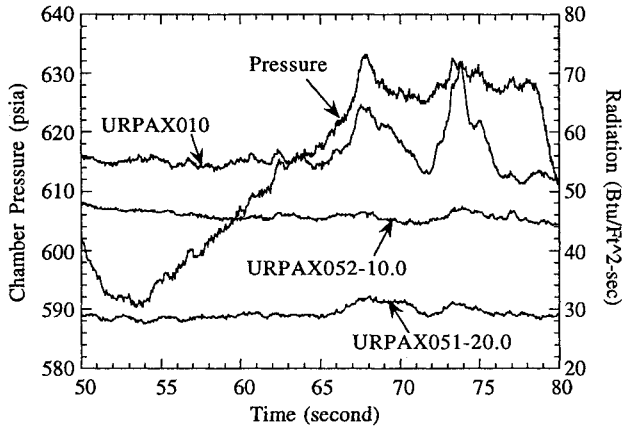

Fig. 9 Comparison of 4-deg narrow-view radiometer measurements in TEM-11 test. Measured fluxes are shifted by increments of 10 Btu/ft^2-s for clarity.

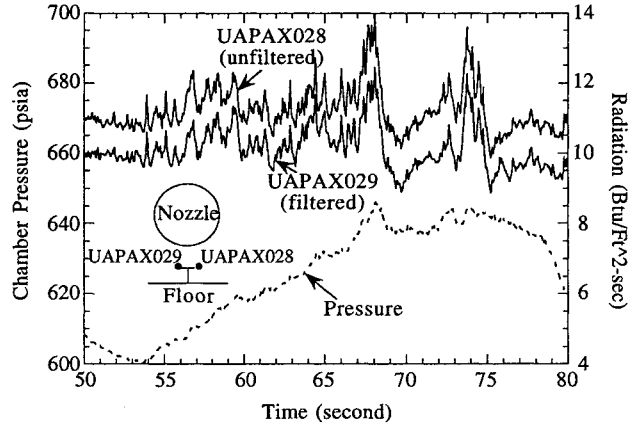

Fig. 10 Radiative flux measured by 50-deg fast-response radiometers in FSM-4 test.

Figure 10 shows the radiation measured by the pair of 50-deg wide-angle radiometers mounted on the test bay floor in the FSM-4 test. The results were similar to other radiometers viewing the plume's bottom half, with definite radiation spikes corresponding to the chamber pressure perturbations. Both the filtered (1.45–1.85 μm) and unfiltered (0.15–5.0 μm) radiometers displayed identical trends in the radiation spikes during the pressure perturbations. This result suggested that the material ejected during the pressure perturbation event could be emitting like a gray body, such as condensed phase aluminum oxide.

The results of the paired radiometers also indicated that a large (over 90%) portion of the radiative heat flux from the plume was in the spectral region with a wavelength of less than 2 μm. Analytical calculations using the reverse Monte Carlo method[13] indicated that nearly 70% of the radiation from the plume was contributed by the aluminum oxide particles with gray-body emission characteristics. Consequently, a large portion of the plume radiation in the spectral region with a wavelength of less than 2 μm is contributed by the condensed phase aluminum oxide, and special attention will be given to the less than 2-μm region of the plume spectrum in the spectrometer investigation proposed for any future RSRM tests. As previously mentioned, efforts to obtain spectral information have been unsuccessful in both the TEM-11 and FSM-4 tests.

Preliminary calculations using a reverse Monte Carlo method[13] indicate that the ratio of the heat flux in the 2-μm region to the heat flux in the 10-μm region will be increased by about 10% during the pressure perturbation events. This increase is caused primarily by the addition of a sheet of liquid slag (aluminum oxide) mass to the plume products according to the reverse Monte Carlo calculation. The temperature of this liquid slag is higher than its surrounding gases, since slag retains its heat better than gas. The Monte Carlo method also predicts that the 10-μm region of the spectrum is not significantly affected by the addition of the slag in the plume. Consequently, any significant change in the plume's spectral content during the pressure perturbation events would have clearly demonstrated the nature of the fluid ejected during such events.

Figures 11a–11d show some frames of the IR images of the plume before, during, and after the 68-s pressure perturbation event in the TEM-11 test. The figure insets indicate the instantaneous chamber pressure corresponding to the thermal image frames shown and radiation flux to the radiometer gauge (UANAV001) located at 22.5 deg on the nozzle external wall. This sequence of thermal images clearly demonstrates the ejection of hot fluid in the plume near the bottom of the nozzle exit plane, coinciding with the 11-psi pressure perturbation in the motor chamber pressure. The ejecta show up as fluid with temperatures significantly higher (Figs. 11b and 11c) than the exhaust gas temperatures in the quiescent plume (Figs. 11a and 11d). Corresponding radiation spikes in the radiometers viewing the bottom of the plume, and the emission of white, hot streaks in the high-speed motion pictures, further confirm this observation. The temperature scale shown in these figures was calculated assuming a plume with an emissivity of one (ε = 1.0). Assuming an average plume temperature of 3640°F (nozzle exit temperature from one-dimensional equilibrium flow calculations using the NASA Lewis code) for the quiescent plume and a measured temperature of 2020°F (with ε = 1.0) from the results of the thermal image, an effective plume emissivity of 0.19 can be calculated using the T^4 law for radiative heat flux. The temperatures shown in the thermal images can be translated to actual plume gas temperatures using this effective plume emissivity. Similar observations were made in the IR motion pictures during other chamber pressure perturbations in the TEM-11 and FSM-4 tests.

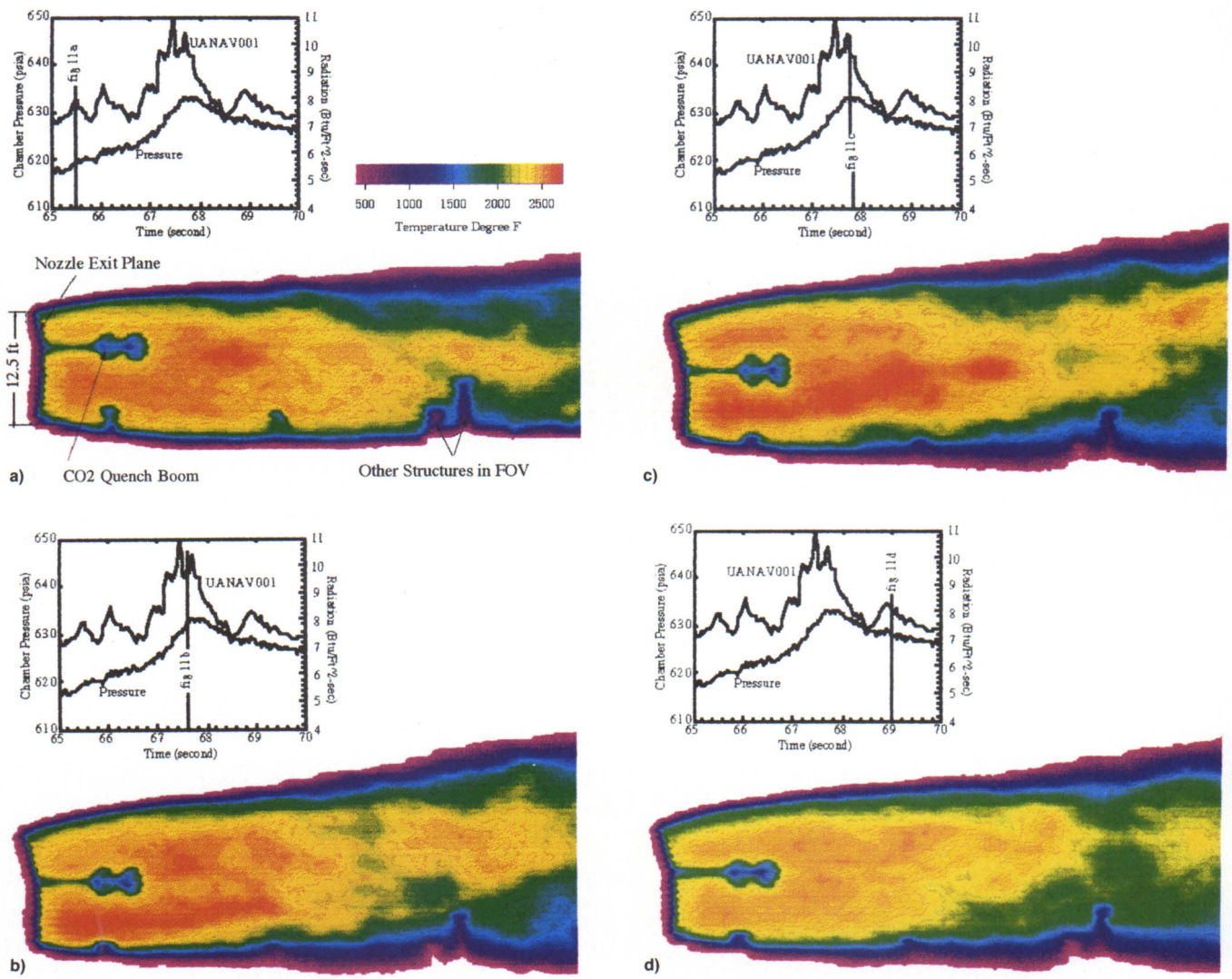

Fig. 11 Plume thermal image at a) 65.5 s (before 11-psi chamber pressure perturbation) in TEM-11. The nozzle is at null position. No unusual hot emissions noticed in plume. (Color scale applies to all following thermal images.) b) Plume thermal image at 67.6 s (during 11-psi chamber pressure perturbation) in TEM-11. Nozzle is vectored at 5.5-deg pitch. Hotter emissions from the ejecta in plume near bottom of the nozzle exit plane. c) Plume thermal image at 67.8 s (during 11-psi chamber pressure perturbation) in TEM-11. Nozzle is vectored at 5.5-deg pitch. Hotter emissions from the ejecta in plume still observed near bottom of the nozzle exit plane. d) Plume thermal image at 69.0 s (after 11-psi chamber pressure perturbation) in TEM-11. Nozzle is vectored at 5.5-deg pitch. No unusual hot emissions observed in plume.

Conclusions

The excellent agreement among all of the nonintrusive optical (high-speed motion pictures) and IR (radiometers and thermal image cameras) observations of the plume during pressure perturbation events in the full-scale SRM static firing tests provides sufficient circumstantial evidence to conclude that the expulsion of slag accumulated inside the motor during the motor burn is the primary cause for the chamber pressure perturbations in the RSRM. The pressure, force, RTR, strain, and accelerometer data[12] obtained during the same tests also support the slag expulsion phenomena. These observations actually show that nozzle vectoring can result in slag expulsion and accompanying pressure perturbations in static motor tests. A deductive conclusion from these observations of the static motor tests may be that even in the absence of significant nozzle vectoring, some other phenomena present in both static and flight motor burns[6,9] also cause slag ejection and associated pressure perturbations.

Acknowledgments

The authors express their most sincere appreciation to the NASA Marshall Space Flight Center employees and the engineers at Thiokol Corporation Space Operations in Utah who provided valuable engineering support before, during, and after the TEM-11 and FSM-4 static tests. This effort would not have been possible without their assistance and cooperation.

References

[1]Ketner, D., and Whitesides, H., "Thermal/Flow Modeling Developed in Support of the RSRM," Session II—STS Solid Rocket Booster, Large Solid Rockets Advances Through Experience AIAA Conf., Monterey, CA, Oct. 1994.

[2]Heister, S., and Landsbaum, E., "Analysis of Ballistic Anomalies in Solid Rocket Motors," AIAA Paper 85-1303, July 1985.

[3]Murdock, J. W., "Rocket Thrust Perturbation from Discharge of an Inert Body," *Journal of Propulsion and Power*, Vol. 2, No. 2, 1986, pp. 117–123.

[4]Lovine, R. L., Baum, J. D., and Levine, J. N., "Ejecta Pulsing of Subscale Solid Propellant Rocket Motors," *AIAA Journal*, Vol. 23, No. 3, 1985, pp. 416–423.

[5]Whitesides, R. H., "RSRM Pressure Perturbation Investigation—Nozzle Slag Ballistics Analysis," Session II—STS Solid Rocket Booster, Large Solid Rockets Advances Through Experience AIAA Conf., Monterey, CA, Oct. 1994.

[6]Schorr, A. A., and Speas, K. J., "Reusable Solid Rocket Motor (RSRM) Pressure Perturbation Characterization—An Overview," AIAA Paper 95-2722, July 1995.

[7]Johnston, W. A., Murdock, J. W., Koshigoe, S., and Than, P. T., "Slag Accumulation in the Titan SRMU," AIAA Paper 94-3287, June 1994.

[8]Salita, M., "Deficiencies and Requirements in Modeling of Slag Generation in Solid Rocket Motors," *Journal of Propulsion and Power*, Vol. 11, No. 1, 1995, pp. 10–23.

[9]Hopson, C., "Space Shuttle Solid Rocket Motor Slag Expulsion Mechanisms," AIAA Paper 95-2725, July 1995.

[10]Whitesides, R. H., Purinton, D. C., Hengal, J. E., and Skelley, S. E., "Effects of Slag Ejection on Solid Rocket Motor Performance," AIAA Paper 95-2724, July 1995.

[11]Rogerson, J. D., "Dynamic Realtime Radioscopy of SRM During Static Firing," AIAA Paper 95-2727, July 1995.

[12]Brennan, M. T., "FSM-4 Pressure Perturbation Status Report," Thiokol Corp., TWR-66133, Brigham City, UT, Feb. 1995.

[13]Nelson, H. F., "Backward Monte Carlo Modeling for Rocket Plume Base Heating," *Journal of Thermophysics and Heat Transfer*, Vol. 6, No. 3, 1992, pp. 556–558.

Color reproductions courtesy of NASA Marshall Space Flight Center